Journal of Power and Energy Engineering, 2025, 13(11), 86-109
https://www.scirp.org/journal/jpee
ISSN Online: 2327-5901
ISSN Print: 2327-588X

Techno-Economic Analysis of Wind and Geothermal Energy for Reverse Osmosis Desalination: A Case Study of Tripoli

Muetaz Mohammed[1,2*], Sulaiman Boghandora[2], Ahmad Belkhair[3]

[1]Department of Mechanical Engineering, King Fahd University of Petroleum & Minerals, Dhahran, Saudi Arabia
[2]Department of Sustainable and Renewable Energy Engineering, Omar Al-Mukhtar University, Al-Byda, Libya
[3]Department of Renewable Energy Technology, Higher Institute of Science and Technology, Al-Byda, Libya
Email: *moutaz.benali@omu.edu.ly

How to cite this paper: Mohammed, M., Boghandora, S. and Belkhair, A. (2025) Techno-Economic Analysis of Wind and Geothermal Energy for Reverse Osmosis Desalination: A Case Study of Tripoli. *Journal of Power and Energy Engineering*, **13**, 86-109.
https://doi.org/10.4236/jpee.2025.1311006

Received: June 11, 2025
Accepted: November 24, 2025
Published: November 27, 2025

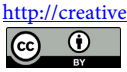

Abstract

Freshwater scarcity, exacerbated by population growth and climate change, is expected to affect most countries by 2050. Desalination has become an essential option in regions facing brackish or seawater shortages, yet its high energy demand underscores the importance of renewable energy integration. This study presents a techno-economic analysis of wind and geothermal energy for powering a reverse osmosis (RO) desalination system in Tripoli, Libya. The RO system was selected as it is the most suitable for medium- and small-scale applications. Using the System Advisor Model (SAM) with the power purchase agreement (single owner) approach, the annual water demand of 100 households 27,375 m^3 was translated into an annual electricity requirement of 68,440 kWh. At small scale, the Levelized Cost of Energy (LCOE) was 41.16 ¢/kWh for wind and 950.51 ¢/kWh for a binary geothermal plant. When scaled to full capacity, the LCOE dropped substantially to 2.93 ¢/kWh and 6.09 ¢/kWh for wind and geothermal, respectively. The flash geothermal configuration was excluded due to inconsistent performance. The findings demonstrate that wind energy is more feasible for meeting small-scale RO desalination needs in Tripoli, while geothermal energy becomes increasingly competitive at larger capacities.

Keywords

Renewable Energy, Reverse Osmosis System, Wind Power Plant, Geothermal Power Plant, LCOE

1. Introduction

Water and energy are gradually becoming scarce nowadays. Though three-fourths of

the globe is covered with water, which is one of the most abundant resources, only 3% of it is freshwater that is suitable for humans, plants, and animals. Approximately 97% of the volume of water on the planet is saline [1]. Due to population growth and climate change, most countries will experience water scarcity by 2050 [2]-[4]. The demand for desalinating seawater is increasing exponentially, while the sources of non-renewable energy are showing ever decreasing trend. Worldwide, there are over 18,000 desalination facilities [5] [6]. The installed desalination capacity worldwide has been seen to have increased gradually between 2010 and the end of 2019 at a pace of roughly 7% annually [7]-[10]. SWRO's anticipated desalination capacity needed to supply the world's water demand by 2030 is 2374 million m^3/day [11]. There are different types of desalination systems such as SSF (Single stage Flash), MSF (Multi-stage Flash), MED (Multi Effect Desalination), SWRO (Seawater Reverse Osmosis), Membrane Distillation, HDH (Humidification Dehumidification) system, ED (Electrodialysis). The desalination process is energy-intensive. An important obstacle to further desalination is the rising cost of water, which is heavily impacted by energy use (about 50% - 60% of total expenses) [12]. Among all technologies, MSF has the most commercial experience with a capacity exceeding 100,000 tons per day [13]. Nowadays, membrane technologies dominate desalination processes; they make up 69% - 73% of all systems installed globally, whereas thermal techniques make up just about 27% [14]. The membranes come in a range of designs and are intended to provide a permeate water of roughly 500 ppm [15]. After the RO process, MSF is currently the second-most widely used desalination method globally [16]. For brackish water, the required pressure for desalination in RO is between 17 and 27 bars, whereas for seawater, it is between 55 and 82 bars [17]. Its installed capacity varies from 0.1 m^3 per day (for domestic and marine uses) to 395,000 m^3 per day (for commercial applications) [14]. In MSF, the energy consumption is particular and ranges from 10 to 16 kWh/m^3, while SWRO consumes 3 - 4 kWh/m^3 [17]. Desalination releases air pollutants into the atmosphere, including greenhouse gases (GHGs), acid rain gases (NO_X; SO_2), and fine particulate matter. This is a major environmental and public health hazard [18]. About 76 million tons (Mt) of carbon dioxide (CO_2) are released each year from desalination plants, and by 2040, that amount is predicted to rise to 218 Mt [19]. So, for producing fresh water, the use of renewable energy has become a sustainable solution. Solar, geothermal, and wind energy are the most widely used renewable energy sources. By 2030, the world's installed PV capacity is expected to have increased over six times, to 2841 GW, from 481 GW in 2018 [20]. Shahbazi *et al.* [21] analyzed the impact of wind turbines on decarbonization and found the amount of carbon dioxide reduction being is more than 31 tons per year in the Firoozkouh area by using a 10 kW wind turbine. Nowadays, energy from renewable sources accounts for only 1% of the total amount of desalinated water produced [21] [22]. Geothermal energy is one of the renewable energy sources that can supply a continuous power requirement, like that of a cogeneration desalination plant, without the need for power storage [23]-[26]. When compared to standard MED, MED with geothermal sources and Hybrid MED with SWRO at 130˚C, 115˚C, and 100˚C as heat sources will save 46%, 85%, 88%, and 89% of electricity consump-

tion, respectively [25]. Kabiri *et al.* used solar energy to repower in an MSF system can result in a GOR of 9.62 with a production rate of 115.4 kg/s [5]. Ghaffour *et al.* developed an adsorption desalination (AD) and membrane distillation (MD) system based on renewable energy systems. To minimize the likelihood of exhausting the heat source within the geothermal reservoir and to maximize the use of RE without the need for energy storage, a novel hybrid approach that combines solar and geothermal energy using an alternating 12-hour cycle that has an energy consumption of < 1.5 kWh/m^3 of water has also been investigated by them [11]. Bozgeyik *et al.* investigated a 10-stage MSF system with a production rate of 5.74 m^3/day, which comprises a parabolic trough collector, an organic Rankine cycle (ORC), and a PEM electrolyzer and heat exchanger as sub-systems, produces hydrogen, power, and hot water for space heating and residential use [12]. Gude *et al.* proposed to utilize low-grade heat sources, such as waste heat or solar energy, to power a low-temperature, low-pressure desalination plant and presented six different ways that the method could be put into practice [13]. Li and Zhang have devised and built a test rig for an HDH desalination system powered by solar energy where the specific energy consumption (solar and electric) by unit volume of water production is less than 924.35 kWh/m^3 (905.12 kWh/m^3 from solar energy and 19.23 kWh/m^3 from electric energy), and the freshwater production rate is greater than 15.27 kg/day [16]. Greco *et al.* reviewed all the recent works on desalination using wind energy both as a backup and standalone [15]. Sayed et summarized the recent progressions of renewable energy engagement in the desalination process in the MENA region and it was discovered that tiny capacity plants were quite expensive, making them less competitive with traditional plants [14]. Yildırım and Solmus [18] conducted a theoretical analysis of the efficiency of a solar-powered HDH desalination process. The analysis considered several working units and the design characteristics specific to Antalya, Turkey's climate. Increasing the air mass flow rate and the feed water mass flow rate had a beneficial effect on the generation of clean water. Their proposed model was estimated to produce 12 tons of fresh water annually. Greco *et al.* proposed a cost table for all types of desalination systems and found that the ED (Electrodialysis) was the cheapest one and SWRO and MSF had maximum output capacity [14]. The MSF unit's overall equivalent energy consumption falls between 19.58 and 27.25 kW he/m^3 [23]. Consequently, the MED units' overall equivalent energy consumption ranges from 14.45 to 21.35 kWh/m^3 [23]. The electrical energy consumption of a brackish-water RO (BWRO) unit is between 1.5- and 2.5-kWh/m^3 [23]. An ED unit's electricity usage ranges from 0.7 to 2.5 kWh/m^3 for low salinity (o2500 ppm) and 2.64 to 5.5 kWh/m^3 for salinity ranges between 2500 and 5000 ppm, respectively [23]. Rafiei *et al.* investigated the effects of various shapes of cavity receivers including hemispherical, cylindrical, and cubical on the performance of an HDH system [17] and found that among all cavity forms, the hemispherical receiver's thermal efficiency and cavity heat gain showed the largest quantity. Mohamed and El-Minshawy [19] modeled an HDH system using geothermal energy and concluded that the practical application of the low enthalpy geothermal energy is accessible at temperatures as high as 100 for application desalination. It was discovered that the range of 1.5 to

2.5 represented the ideal value for the ratio of seawater mass flow rate to air mass flow rate. According to research, nuclear desalination plants can produce 80 - 100 or 200 - 500 km^3 of desalinated water each day [19]. It is anticipated that the related costs for RO will be 50 - 94 ¢/m^3, MED will be 60 - 96 ¢/m^3, and MSF plants will be 1.18 - 1.48 \$/m^3 using nuclear energy [19]. When comparing the energy consumption of the three most used seawater desalination procedures (MED, RO, and MSF), we find that the RO process uses less energy than the distillation processes (MED and MSF).In comparison to 4 to 6 kWh/m^3 of water for the SWRO process with an ER system, it is approximately 19.58 to 27.25 kWh/m^3 of water for MSF and 14.45 to 21.35 kWh/m^3 of water for MED [11]. The overall performance and comparison of major desalination technologies are summarized in **Table 1**.

In this study, the problem addressed is freshwater scarcity and the high energy demand of desalination, which requires sustainable solutions. RO is an efficient technology, but its feasibility strongly depends on the cost of energy. Wind and geothermal power are promising renewable sources; however, there is a lack of techno-economic analysis to determine which option is more feasible for running RO desalination. This challenge is faced across Libya, where water resources are under severe stress due to over-extraction and limited natural recharge. The problem is particularly acute in the major cities, such as Tripoli, which is the largest and most densely populated city in the country. Tripoli currently relies heavily on deep groundwater extraction through the Great Man-Made River project, but with rising demand and declining reserves, the city is projected to face serious water shortages by 2050 [27]. Under such circumstances, Libya in general—and Tripoli in particular—will increasingly need to rely on the desalination of brackish and seawater to meet demand, with the average per capita water requirement estimated at 150 liters/day [28].

Table 1. Capacity & power consumption by major desalination technologies [11]-[14].

Properties	MSF	MED	MVC	TVC	SWRO	BWRO	ED
Typical unit size (million m^3/day)	50 - 70	5 - 15	up to 3	10 - 30	Up to 128	Up to 98	Up to 145
Electrical energy consumption (kW h/m^3)	2.5 - 5	2 - 2.5	7 - 12	1.8 - 1.6	4 - 6	1.5 - 2.5	2.64 - 5.5
Thermal energy consumption (MJ/m^3)	190 - 282	145 - 230	None	227	None	None	None
Equivalent electrical to thermal energy (kW h/m^3)	15.83 - 23.5	12.2 - 19.1	None	14.5	None	None	None
Total electricity consumption (kW h/m^3)	19.58 - 27.25	14.45 - 21.35	7 - 12	16.26	4 - 6	1.5 - 2.5	2.64 - 5.5
Product water quality (ppm)	≈ 10	≈ 10	≈ 10	≈ 10	400 - 500	200 - 500	150 - 500

2. Energy Requirement

According to the Libya Bureau of Statistics, in 2022, data on the average household size of Tripoli was reported to be 5 persons. The least energy consumption is by BWRO, and it is 1.5 - 2.5 kWh/m^3 [23]. From the literature, if we consider the average family size consisting of 5 people, the annual water consumption of 100 households can be calculated by

Annual water consumption = Water consumption per capita × Average House-

hold Members × Number of Household × Days in a Year = 0.150 × 5 × 100 × 365 = 27,375 m^3.

Total amount of electricity required annually = Energy required per kWh × Total water required = 2.5 × 27,375 ≈ 68,440 kWh.

The monthly requirement is nearly 4,791 kWh. When considering the RO plant at full capacity, it produces 1000 – 3.2 × 10^5 m^3 per day [7]. We assume an average output of 1.0 × 10^5 m^3 per day. This corresponds to an annual production of 3.65 × 10^7 m^3. The energy requirement at full capacity is therefore calculated as 2.5 × 3.65 × 10^7 = 9.125 × 10^7 kWh resulting in a monthly requirement of approximately 7.6 × 10^6 kWh.

3. Methodology

This study employed the SAM [29] to estimate wind energy output using various turbine configurations and their associated characteristics. The primary advantage of SAM is its user-friendly interface, which makes it an effective tool for beginners to simulate renewable energy systems such as solar and wind power. Moreover, SAM is capable of modeling enhanced geothermal systems, including both flash and binary conversion plants that utilize hydrothermal resources [25]. In this analysis, the contributions of geothermal and wind energy are examined and compared.

3.1. Wind Power Plant

A typical schematic diagram of a wind turbine-driven desalination plant, incorporating both backup and storage systems, is illustrated in **Figure 1**.

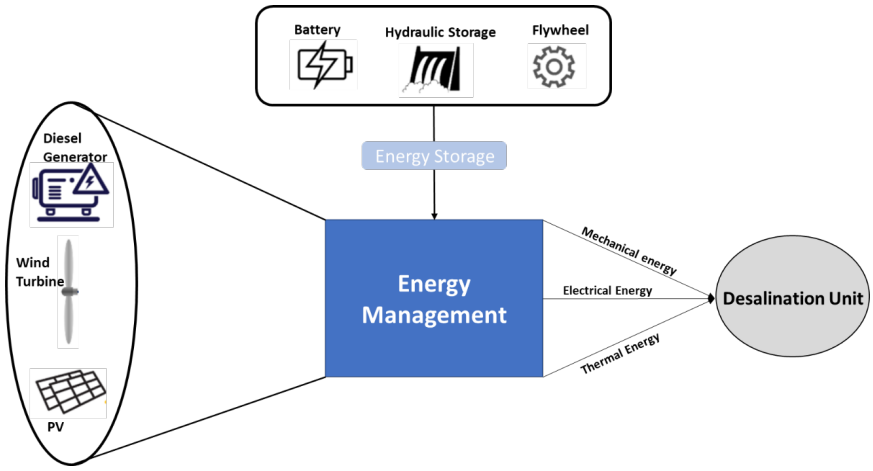

Figure 1. Desalination plant primarily powered by a wind turbine, with additional backup sources [15].

SAM also provides a collection of built-in locations. However, since Tripoli is situated at an elevation of approximately 81 m above sea level, with coastal zones at lower altitudes, the region generally exhibits moderate to low wind speeds. Therefore, selecting a location significantly different from Tripoli would not realistically represent the city's actual wind conditions for the design of a wind turbine

plant. Consequently, the Tripoli site was adopted as the reference location within SAM. Several wind turbine models were utilized as input parameters in the software, and the subsequent analysis of power output and the LCOE for turbines falling within the target output range is presented in Table 2.

Table 2. Comparison of wind turbines based on quantity, energy output, and LCOE.

Turbine name	Number of turbines	Average monthly output (kWh)	LCOE (¢/kWh)
Wind spot 7.5 kW 6.3 m	3	4600	55.16
Bergey Excel - S.60	2	6000	41.16
Aircon10 S 7.54 10 kW	2	6500	38.78
Evoco 10 kW 9.7 m	2	7000	35.99
Gaia wind 133- 11 kW	2	8000	32.57

Based on the data presented in Table 2, the most suitable wind turbine for our analysis in terms of power demand is the Bergey Excel-S.60. Although this turbine exhibits a slightly higher LCOE compared to the other three models, its average monthly power output closely matches the required energy demand. Therefore, the Bergey Excel-S.60 was selected for further performance assessment, and the detailed simulation and economic analysis are presented in Table 3.

Table 3. Overall statistical data of bergey excel - s.60 wind turbine plant.

Metric	Value
Annual AC energy in Year 1	75,161 kWh
Capacity	20 kW
Capacity factor in Year 1	42.9%
PPA price in Year 1	4.00 ¢/kWh
PPA price escalation	1.00 %/year
LPPA Levelized PPA price nominal	4.33 ¢/kWh
LPPA Levelized PPA price real	3.44 ¢/kWh
LCOE Levelized cost of energy nominal	51.84 ¢/kWh
LCOE Levelized cost of energy real	41.16 ¢/kWh
NPV Net present value	$–349,023
IRR Internal rate of return	NaN
Year IRR is achieved	20
IRR at end of project	–11.71 %
Net capital cost	$482,386
Equity	$460,963
Size of debt	$21,423
Debt percent	4.44%

From the statistics, the LCOE is observed to be 51.84 ¢/kWh, while the net capital cost amounts to $ 482,386. The LCOE could have been lower if both the system capacity and the annual AC energy generation were higher. However, the elevated LCOE in this case is primarily attributed to the relatively low power demand.

3.2. Geothermal Power Plant

Geothermal energy can be effectively harnessed for desalination by utilizing the earth's internal heat to drive the evaporation and condensation processes required to produce fresh water from seawater. In a geothermal desalination plant, geothermal wells extract hot fluids from underground reservoirs, which are then used to heat saline water. The heated water undergoes evaporation, and the resulting steam is condensed into fresh water, while the concentrated brine is discharged or further treated. This process provides a sustainable and energy-efficient alternative to conventional desalination methods, especially in regions with abundant geothermal resources. The schematic layout of this system is illustrated in Figure 2.

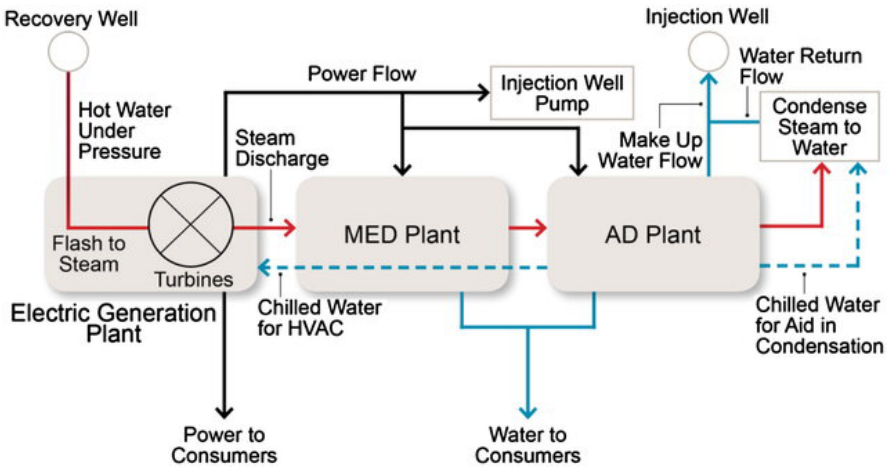

Figure 2. Schematic diagram of a geothermal desalination plant, where geothermal energy is used to generate electricity through turbines and steam flow, which is then supplied to MED and RO plants. The treated water undergoes post-treatment before being delivered to consumers, while excess electricity is distributed to external users [11].

The resource potential, plant output, and number of wells were determined based on the annual energy demand for desalination. During this assessment, it became evident that for such relatively low requirements, the LCOE and the IRR yielded poor and unrealistic values. This indicated that an increase in plant capacity and output would be necessary to generate more reliable and economically viable data. The LCOE was calculated to be approximately 950.51 ¢/kWh; however, this value was reduced by decreasing the well depth to 600 m. Despite this adjustment, the combination of low power output and limited system requirements continued to pose challenges, as the elevated LCOE undermines the project's feasibility. Simulation analysis in the SAM further revealed that increasing the plant's output and

resource potential leads to significant variations in the LCOE. The projected annual AC energy generation was approximately 87,067 kWh, or 7256 kWh per month, which exceeds the estimated demand. Nonetheless, it was also observed that over time, the well temperature and output potential decline. Therefore, this output level was considered adequate to ensure that the system could meet demand over a 25-year operational lifetime.

4. Results and Discussion

The simulation study for both the wind turbine and the geothermal plant encompassed a detailed examination of the input parameters, the technical and economic considerations, as well as the resulting performance outcomes. In this context, the parameters define the operational boundaries and assumptions applied during the modeling process, such as resource availability, system capacity, efficiency levels, and expected lifetime of the technologies. The considerations include the external and internal factors that may influence the accuracy and reliability of the results, for example, site-specific resource variability, equipment limitations, and economic constraints related to investment and operation. Finally, the results summarize the key findings obtained from the simulations, including projected energy outputs, efficiency levels, cost metrics, and long-term sustainability indicators. By presenting the parameters, considerations, and results together, a comprehensive understanding of the wind turbine and geothermal plant performance under the given conditions is established.

4.1. Wind Power Plant

The wind turbine selected for this study is the Bergey Excel-S.60, which has a rated power output of 10 kW, a rotor diameter of 6 meters, and a hub height of 80 meters. The turbine begins operation at a cut-in wind speed of 3 m/s, reaches its rated output at 14 m/s, and shuts down at a cut-out speed of 21 m/s. Simulation results indicate an annual AC energy generation of 87,067 kWh in the first year, with a remarkably high-capacity factor of 99.4%. The PPA price in the first year is estimated at 8.00 ¢/kWh with a 1% annual escalation, while the LPPA price is 8.60 ¢/kWh nominal and 6.95 ¢/kWh real. On the other hand, the LCOE is significantly higher, calculated at 1175.99 ¢/kWh nominal and 950.51 ¢/kWh real, highlighting economic challenges for small-scale deployment. The NPV is negative at $8,842,039, and IRR could not be achieved over the project lifetime, with the year IRR is achieved projected only by year 20. The total net capital cost is estimated at $12,029,998, with equity contributions of $13,648,896 and a debt size of −$1,618,898, resulting in an unusual negative debt percentage of −13.46%. These findings emphasize the technical viability of the turbine for energy generation but also reveal substantial economic limitations under the given assumptions.

The variation of wind speed over different months of the year provides valuable insights into the seasonal behavior of the wind resource at the study location. As

shown in the monthly profiles, wind speeds generally fluctuate between 8 - 11 m/s, with noticeable dips during the summer months (June to August) and relatively higher stability during the winter and early spring. This seasonal variation directly influences the annual energy yield and highlights the importance of accounting for temporal changes in wind patterns when designing and evaluating wind energy systems. The overall annual profile further illustrates the average trend across the year, confirming that the site maintains sufficient wind resources to support turbine operation throughout the year. The detailed monthly and annual wind speed variations are presented in Figure 3.

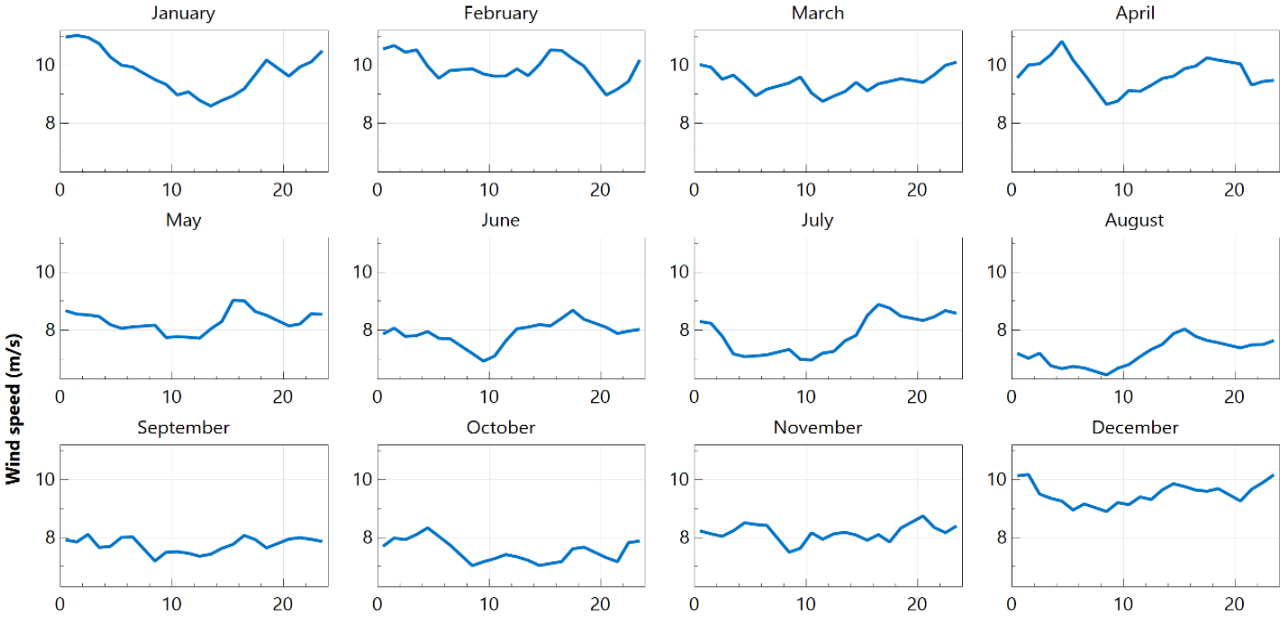

Figure 3. Monthly and annual wind speed profiles at the study site, showing seasonal variations and average annual wind distribution.

The statistical distribution of wind speeds at the study site was analyzed to assess the frequency and probability of occurrence, which is critical for accurately estimating the expected energy yield of the turbine. The histogram illustrates the percentage of data points for different wind speed ranges, while the cumulative distribution curve provides the corresponding probability distribution. The analysis shows that the most frequent wind speeds fall within the range of 6 - 10 m/s, with a median wind speed (P50) of approximately 8.24 m/s. This indicates that the site has a reliable wind resource suitable for continuous energy generation. Such information is essential for evaluating turbine performance, predicting annual energy production, and reducing uncertainty in project planning. The wind speed distribution and cumulative probability are presented in Figure 4.

The system power output distribution was analyzed to evaluate the expected energy generation capacity of the wind turbine under varying operating conditions. The histogram illustrates the frequency of different power outputs, while the cumulative curve indicates the probability of achieving or exceeding a given

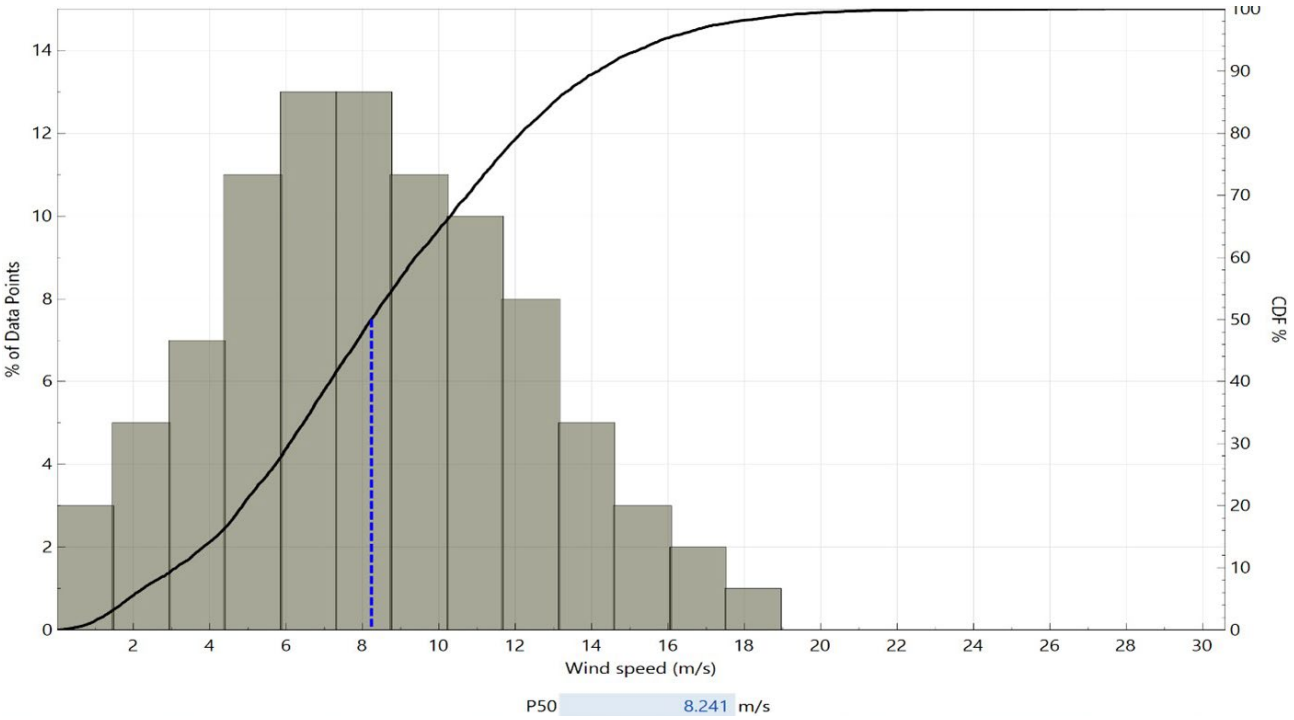

Figure 4. Wind speed frequency distribution and cumulative probability curve at the study site, indicating a median (P50) wind speed of 8.24 m/s.

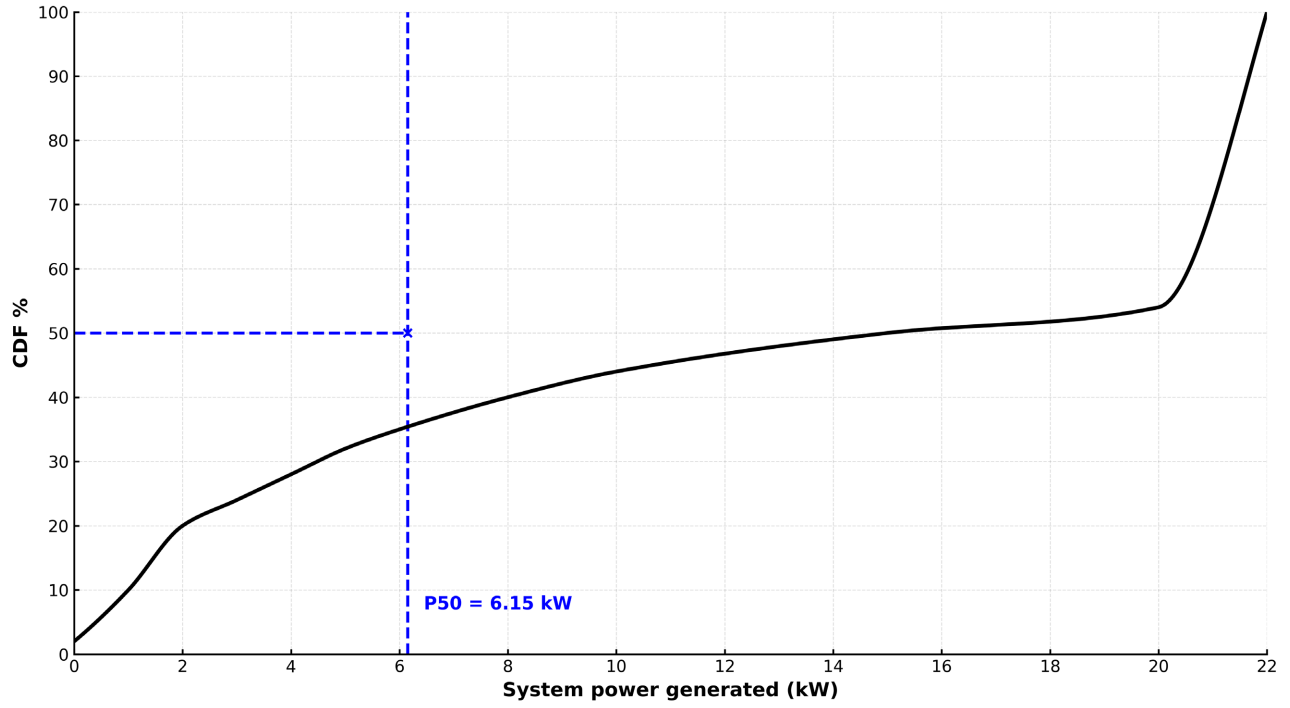

Figure 5. Distribution of system power output with cumulative probability curve, showing a median (P50) power generation of 6.15 kW.

output level. The analysis shows that the turbine most frequently operates within the lower to mid-power range, with a median (P50) power generation of approximately 6.15 kW. Although the system is capable of reaching higher outputs close

to its rated capacity (20 kW), such events occur less frequently due to the dependence on higher wind speeds. This statistical evaluation provides a realistic estimate of the turbine's operational performance and energy contribution over time, which is crucial for project feasibility assessments and long-term planning. The power generation distribution and cumulative probability are presented in Figure 5.

The monthly AC energy output during the first year of operation provides a clear picture of the seasonal variations in turbine performance. As shown in the figure, energy generation peaks in January at over 8000 kWh, reflecting strong winter wind resources. Relatively high outputs are also observed during February through April, maintaining values above 7000 kWh. However, from May onwards, a gradual decline is observed, with the lowest output occurring in August at around 4500 kWh, corresponding to weaker summer wind speeds. The production then begins to recover from September, reaching another peak in December with approximately 7300 kWh. These fluctuations highlight the direct influence of seasonal wind speed variability on turbine performance and demonstrate the importance of annual resource assessment to ensure reliable energy supply. The detailed monthly AC energy generation profile for Year 1 is illustrated in Figure 6.

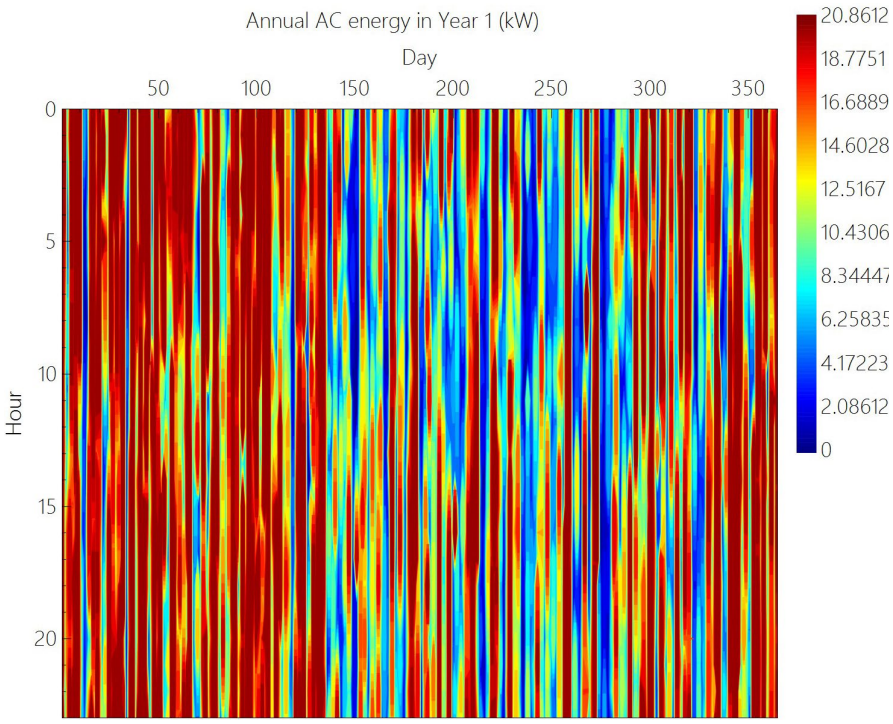

Figure 6. Monthly AC energy generation in the first year, showing seasonal variation in wind turbine output with peak production in winter months and reduced output during summer.

The annual AC energy profile provides a detailed hourly and daily distribution of power generation throughout the first year of operation. As illustrated

in the figure, energy production fluctuates significantly across both seasonal and diurnal cycles, reflecting variations in wind resource availability. High power outputs, shown in red, are more concentrated during certain periods, particularly in the early and late months of the year, corresponding to stronger winter and autumn winds. Conversely, lower outputs, represented by blue shades, are more frequent around the mid-year period, aligning with the weaker summer wind conditions identified in earlier analyses. This heatmap-style representation highlights not only the variability of wind power generation but also the turbine's capacity to deliver substantial energy output during peak wind periods. Such insights are crucial for understanding resource intermittency, planning energy storage or backup systems, and ensuring reliable integration into desalination operations. The hourly and daily distribution of annual AC energy in Year 1 is shown in Figure 7.

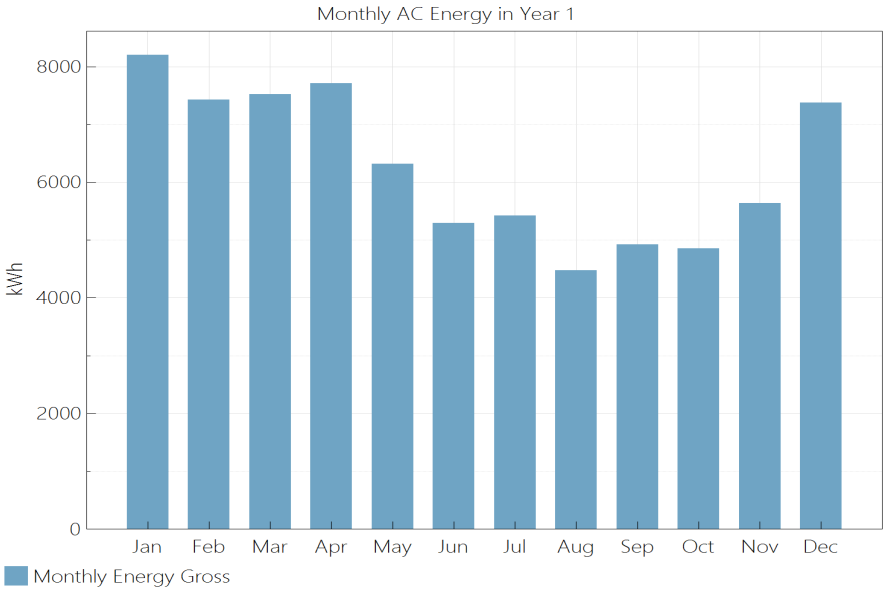

Figure 7. Heatmap of annual AC energy generation in the first year, showing hourly and daily variations in turbine output, with higher production in winter and lower production in summer.

The long-term projection of electricity generation demonstrates the consistency of the wind turbine's performance over its operational lifetime. As shown in the figure, the annual net generation remains relatively stable at around 74,000 - 75,000 kWh for each year across the 25-year period. This indicates that the system is capable of sustaining a steady energy output over the long term, with minimal performance degradation considered in the simulation. Such stability is critical for supporting desalination operations, where continuous and reliable electricity supply is essential. Furthermore, the consistent output enhances the predictability of energy availability, which plays an important role in economic assessments and planning for system integration. The projected net electricity generation over 25 years is illustrated in Figure 8.

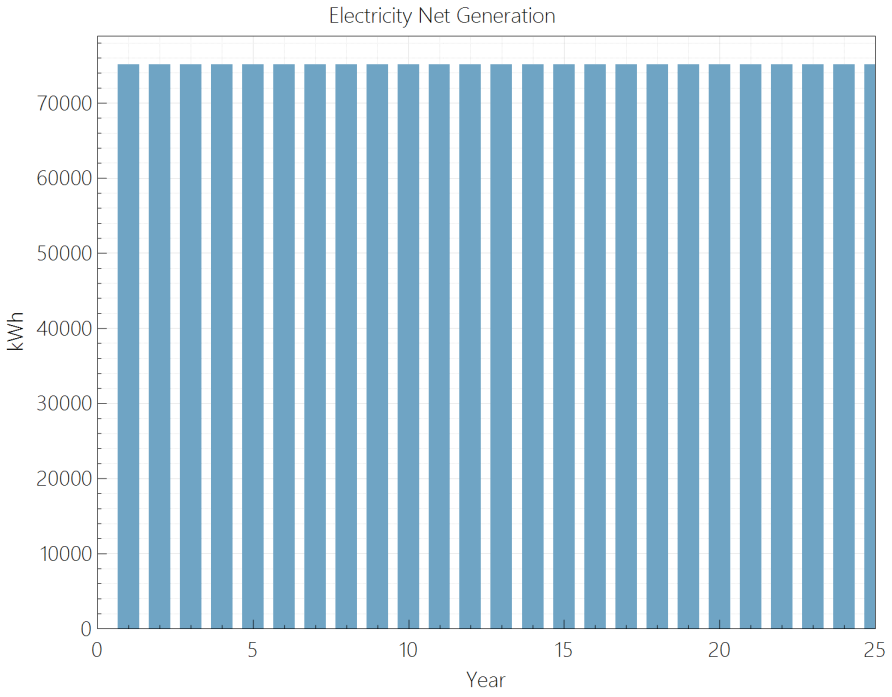

Figure 8. Projected electricity net generation of the wind turbine system over 25 years, showing stable long-term performance with annual outputs averaging around 74,000 - 75,000 kWh.

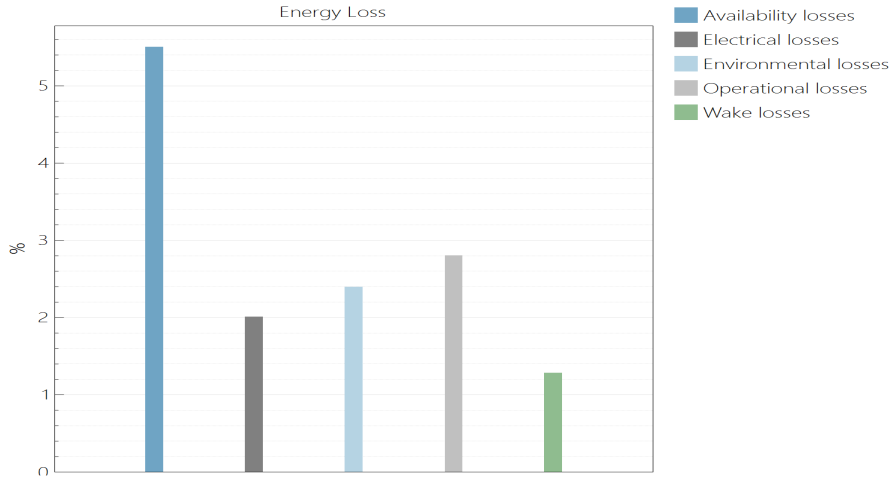

Figure 9. Breakdown of energy losses in the wind turbine system, showing availability losses as the dominant factor followed by operational, environmental, electrical, and wake losses.

The analysis of system energy losses highlights the different factors contributing to reductions in overall efficiency. As illustrated in **Figure 9**, availability losses are the most significant, accounting for more than 5% of total losses, followed by operational losses at nearly 3%. Availability losses arise from non-operational hours of the turbine or the plant, which may be due to scheduled maintenance, unexpected failures, or other interruptions. Operational losses, on the other hand, occur during turbine operation and are primarily caused by aerodynamic inefficien-

cies such as drag on the rotor blades and tip losses. Electrical losses, which represent about 2% of the total, are associated with inefficiencies in the generator and other electrical components, including wiring and energy conversion processes. Environmental losses contribute approximately 2.4%, while wake losses are relatively minor at about 1.2%. These findings emphasize that while wake and electrical effects are less critical, improvements in system availability and operational performance could substantially enhance overall energy output.

4.2. Geothermal Power Plant

The geothermal plant considered in this study is located in Tripoli and utilizes hydrothermal resources for power generation. The system is designed with a conversion type that incorporates both binary and flash technologies, enabling efficient extraction and utilization of geothermal energy. The total resource potential at the site is estimated to be 10 MW; however, the plant output is limited to 10 kW, reflecting the relatively small-scale scope of the project. The plant configuration includes a single production well with a depth of 600 meters, which serves as the primary source of geothermal fluids. This setup provides the necessary baseline information for evaluating the technical feasibility, operational performance, and long-term sustainability of the geothermal system under the given conditions.

4.2.1 Binary Geothermal Power Plant

The performance analysis of the binary geothermal plant was further evaluated using different simulation outputs to better understand its energy generation characteristics. **Figure 10(A)** presents the system power generation distribution, which indicates that the plant consistently operates within a narrow range, with a median (P50) power output of approximately 8.3 kW, reflecting the stable nature of geothermal resources. **Figure 10(B)** shows the monthly AC energy profile for the first year, where a gradual decline is observed from around 7,200 kWh at the beginning of the year to approximately 5000 kWh by the end, suggesting slight reductions in performance due to operational and resource-related factors. **Figure 10(C)** illustrates the hourly distribution of annual AC energy, which demonstrates a uniform output pattern throughout the day and across the months, confirming the baseload nature of geothermal power generation. Finally, **Figure 10(D)** presents a heatmap of annual AC energy generation, showing minimal variation, with outputs remaining consistently close to the rated capacity of 10 kW. Together, these results confirm the reliability and stability of geothermal energy as a continuous power source, while also highlighting the need to account for minor long-term performance declines in planning and operation.

The long-term electricity generation profile of the geothermal plant highlights the gradual decline in output over its 25-year operational lifetime. As illustrated in **Figure 11**, the net generation begins at approximately 88,000 kWh in the initial year and decreases steadily to about 56,000 kWh by the end of the project period. This reduction is primarily attributed to the natural decline in reservoir temperature and resource potential over time, which directly impacts the system's efficiency and out-

put capacity. Such a trend underscores the importance of accounting for geothermal reservoir depletion in performance assessments and financial planning, as the diminishing energy output affects both technical reliability and economic viability.

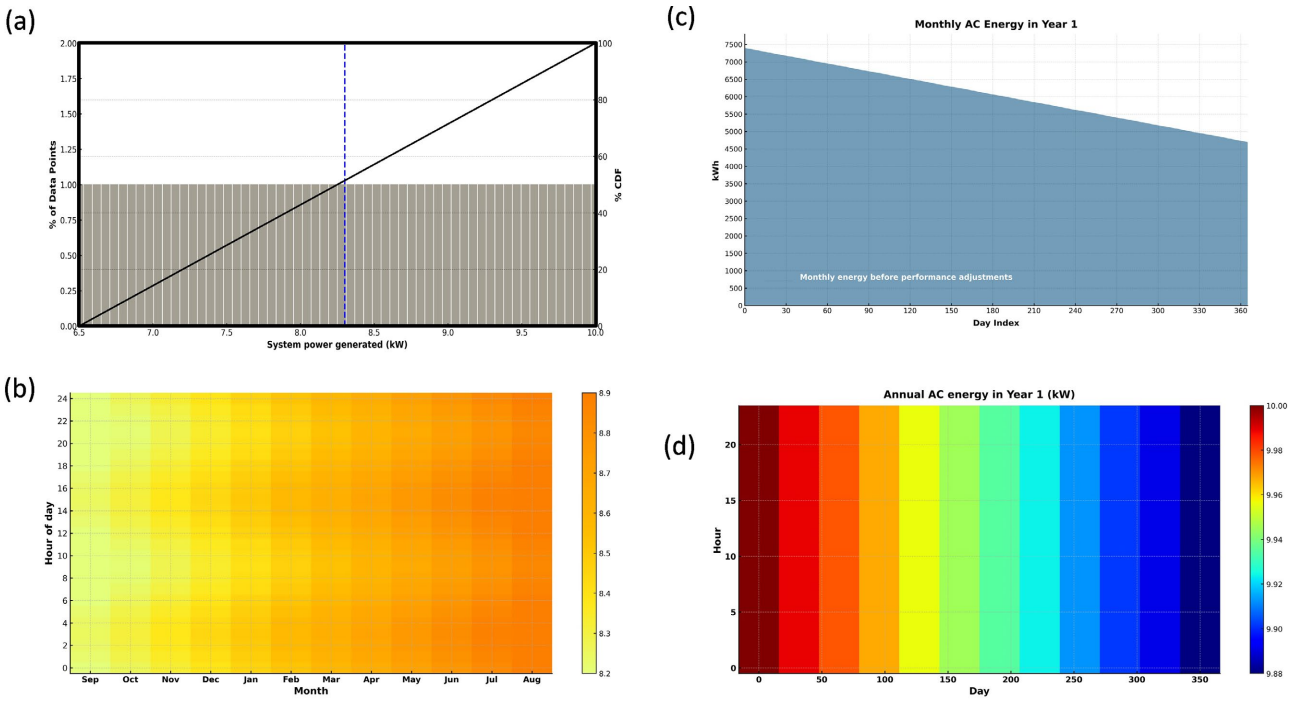

Figure 10. Simulation results of binary geothermal plant performance showing: (a) system power generation distribution, (b) monthly AC energy in Year 1, (c) hourly AC output profile across the year, and (d) heatmap of annual AC energy generation.

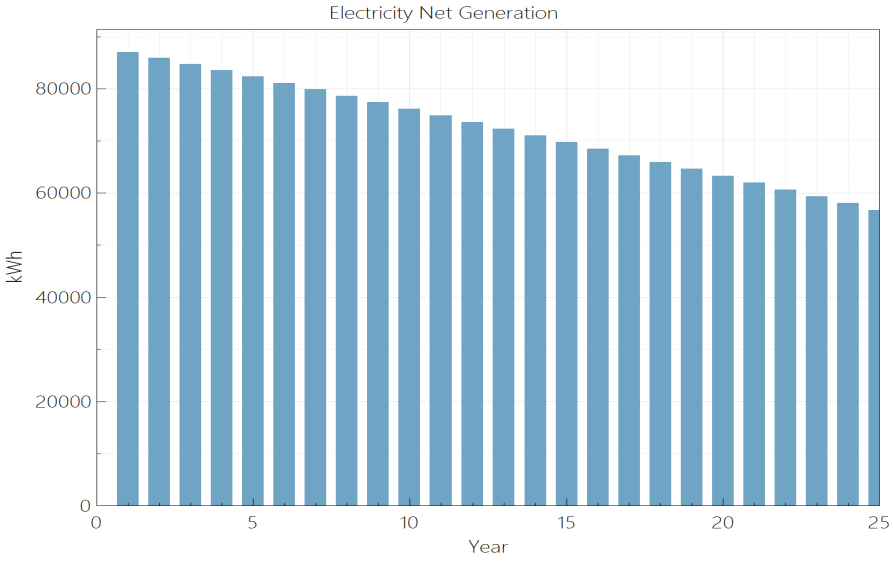

Figure 11. Projected electricity net generation of the binary geothermal power plant over 25 years, showing a gradual decline from about 88,000 kWh in Year 1 to around 56,000 kWh by the end of the project lifetime.

4.2.2. Flash Geothermal Power Plant

The performance assessment of the flash geothermal plant indicates an annual AC

energy generation of 87,140 kWh in the first year, with a capacity factor of 99.5%. The PPA price in Year 1 was estimated at 8.00 ¢/kWh with an annual escalation rate of 1%. The Levelized PPA price was calculated at 8.61 ¢/kWh nominal and 6.94 ¢/kWh real. However, the LCOE was found to be significantly higher, with values of 1158.12 ¢/kWh nominal and 933.85 ¢/kWh real, highlighting economic challenges. The NPV is negative at $8,847,953, while the IRR was not achieved throughout the project lifetime, although the model projects IRR could be reached only after year 20. The total net capital cost is estimated at $12,040,167, with equity contributions of $13,659,188 and a debt size of −$1,619,021, resulting in a negative debt percentage of −13.45%. These results suggest that while the geothermal flash system demonstrates stable technical performance and high reliability in terms of energy output, the economic indicators remain unfavorable under the assumed project conditions.

The flash geothermal power plant performance over time is illustrated in **Figure 13**. As shown in **Figure 12(A)**, the monthly AC energy generation in the first year starts at approximately 7,300 kWh and gradually decreases to about 5,000 kWh by the end of the year, indicating a decline in output due to performance adjustments and resource constraints. **Figure 12(B)** presents the annual AC energy distribution on an hourly and daily basis, which shows consistently high output levels near the rated capacity of 10 kW during the early months, followed by a gradual reduction toward the end of the year. This pattern reflects the long-term stability of geothermal energy while accounting for resource depletion effects. Finally, **Figure 12(C)** demonstrates the net electricity generation trend over a 25-year project lifetime, where annual generation decreases steadily from around 87,000 kWh in the initial year to nearly 60,000 kWh by the end of the period. These results emphasize that while geothermal flash systems provide reliable baseload energy, careful consideration of reservoir decline and efficiency losses is essential for long-term operational and economic planning.

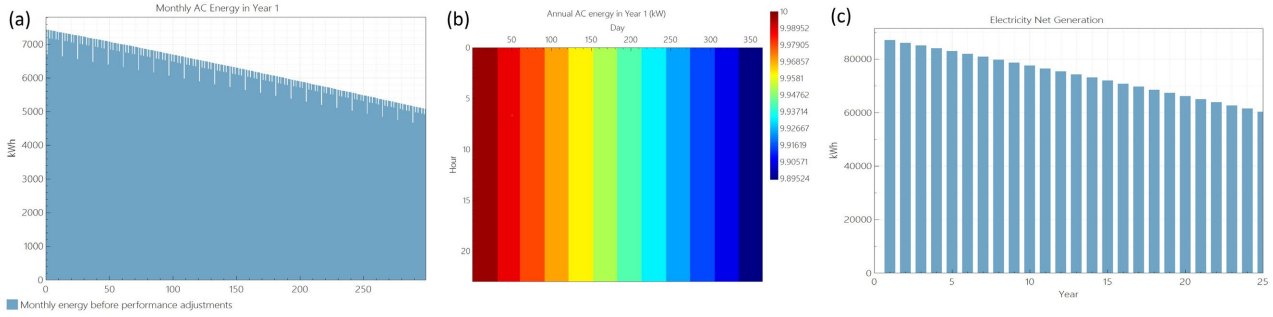

Figure 12. Flash geothermal power plant performance: (a) monthly AC energy in Year 1, (b) annual AC energy distribution, and (c) long-term electricity net generation over 25 years.

From the above results, it can be observed that the annual AC energy outputs of both the flash and binary geothermal power plant are nearly identical, with the flash technology showing slightly higher production. The hourly heat maps for the two systems are also virtually the same, reflecting similar operational behavior

under comparable conditions. However, a distinction emerges in the economic performance: the LCOE for the binary technology is 950.51 ¢/kWh, whereas for the flash technology it is slightly lower at 933.85 ¢/kWh, despite both systems being modeled with the same inputs and capacity. This indicates that, under the given assumptions, the flash configuration provides a marginal economic advantage over the binary technology.

4.3. Assessment of Wind and Geothermal Power Plants at Full Capacity

To better understand the technical and economic feasibility of renewable energy integration, both the wind power plant and the geothermal power plant were evaluated under full-capacity operating conditions. This assessment allows for a direct comparison of their maximum generation potential, resource utilization, and long-term sustainability. By analyzing key parameters such as annual AC energy output, efficiency, and LCOE, the study provides insights into how each system performs when fully utilized. Such an evaluation is essential for determining the suitability of these technologies in meeting continuous energy demand, particularly for energy-intensive applications such as desalination.

4.3.1. Wind Power Plant

For the assessment of wind energy at full capacity, the Bergey Excel-S.60 turbine was deemed unsuitable due to its limited generation capability, and therefore a Siemens 3.6 MW wind turbine with a hub height of 120 m was selected. This turbine is better suited for large-scale power generation, offering more robust performance metrics under full-capacity operation. The technical specifications indicate a cut-in velocity of 3 m/s, a rated velocity of 15 m/s, and a cut-out velocity of 25 m/s, ensuring efficient performance across a wide range of wind conditions. The plant configuration includes a total of nine turbines, which collectively contribute to an impressive annual generation capacity of 102,091,896 kWh. Furthermore, the LCOE was calculated at 2.93 ¢/kWh, demonstrating a significant improvement in economic feasibility compared to small-scale turbines. These results confirm that the Siemens 3.6 MW turbine provides both the technical robustness and economic efficiency required for large-scale wind power applications.

Figure 13 illustrates the operational and performance characteristics of the Siemens 3.6 MW wind turbine under full-capacity conditions. As depicted in Figure 13(A), the turbine's power curve shows that electricity generation commences at a cut-in wind speed of approximately 3 m/s and increases sharply with higher wind velocities. The turbine achieves its rated power output of 3,500 kW at around 15 m/s, maintaining this level of production until the cut-out speed of 25 m/s. This performance pattern demonstrates the turbine's robust aerodynamic efficiency and its capacity to sustain optimal power generation across a broad wind speed range, making it highly suitable for large-scale energy applications.

The monthly variation in AC energy generation during the first operational year is presented in Figure 13(b). The generation profile reveals clear seasonal

dynamics, with elevated outputs in the winter months—particularly January and December—driven by stronger and more consistent wind conditions, while reduced production levels are observed in the late summer period from July to September. These fluctuations reflect natural wind resource variability and highlight the importance of seasonal assessment in project performance forecasting. The comprehensive financial and operational indicators, including key parameters such as (LCOE), (PPA) pricing, and investment returns, are summarized in Table 4, confirming the project's strong technical feasibility and economic viability.

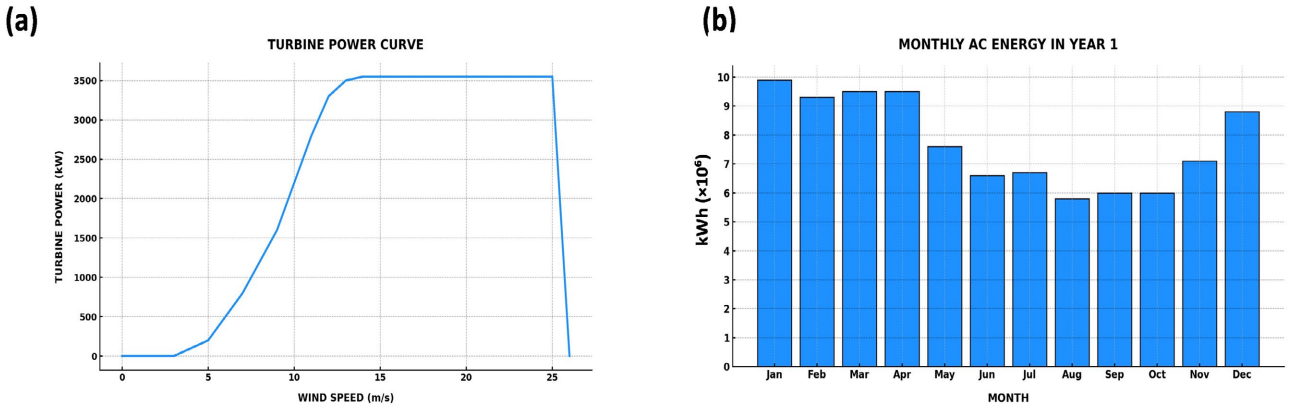

Figure 13. Performance of the Siemens 3.6 MW wind turbine: (a) turbine power curve, (b) monthly AC energy generation in Year 1.

Table 4. Summary of the key financial and performance indicators for the Siemens 3.6 MW wind turbine project, including energy yield, cost metrics, and investment parameters. The results show a strong balance between technical efficiency and economic feasibility, with competitive LCOE values and favorable financial returns.

Metric	Value
Annual AC energy in Year 1	102,091,896 kWh
Capacity	32,400 kW
Capacity factor in Year 1	36.0%
PPA price in Year 1	4.00 ¢/kWh
PPA price escalation	1.00 %/year
LPPA Levelized PPA price nominal	4.33 ¢/kWh
LPPA Levelized PPA price real	3.44 ¢/kWh
LCOE Levelized cost of energy nominal	3.69 ¢/kWh
LCOE Levelized cost of energy real	2.93 ¢/kWh
NPV Net present value	6,424,907$
IRR Internal rate of return	13.46%
Year IRR is achieved	20
IRR at end of project	14.03%
Net capital cost	52,385,508$
Equity	25,942,264$
Size of debt	26,443,246$

4.3.2. Geothermal Power Plant

The geothermal power plant at full capacity is designed to operate at the same location but on a different scale, reflecting the potential of hydrothermal resources when developed beyond small-scale deployment. In this configuration, the system employs both binary and flash conversion technologies to optimize energy extraction. The total resource potential is estimated at 50 MW, with a plant output of 13,000 kW supported by two production wells. Compared to the earlier small-scale system, this larger setup demonstrates how capacity expansion at the same site can significantly enhance energy generation and improve the overall feasibility of geothermal utilization.

As illustrated in Figure 14, the binary geothermal power plant operating at full capacity demonstrated a robust and stable energy generation performance during its first operational year, reaching a total annual AC energy output of 106,853,512 kWh with a capacity factor of 93.8%. The monthly AC energy profile shows a gradual decline over time, reflecting minor operational and thermal variations but maintaining overall consistency and reliability in energy production. This stable generation pattern highlights the technical robustness of the binary configuration and its suitability for sustained geothermal energy extraction. Furthermore, as summarized in Table 5, the plant achieved substantial economic performance, with a significant reduction in the LCOE to 6.09 ¢/kWh (real) and a strong NPV of $9.9 million, supported by an IRR of 32.02% by Year 20. The total capital cost of $62.86 million, financed primarily through a 67.92% debt ratio, demonstrates an optimal balance between investment scalability and financial return. Together, Figure 14 and Table 5 confirm that the full-scale binary geothermal power plant configuration offers a compelling combination of high technical efficiency and strong economic feasibility, establishing it as a viable model for large-scale geothermal energy development.

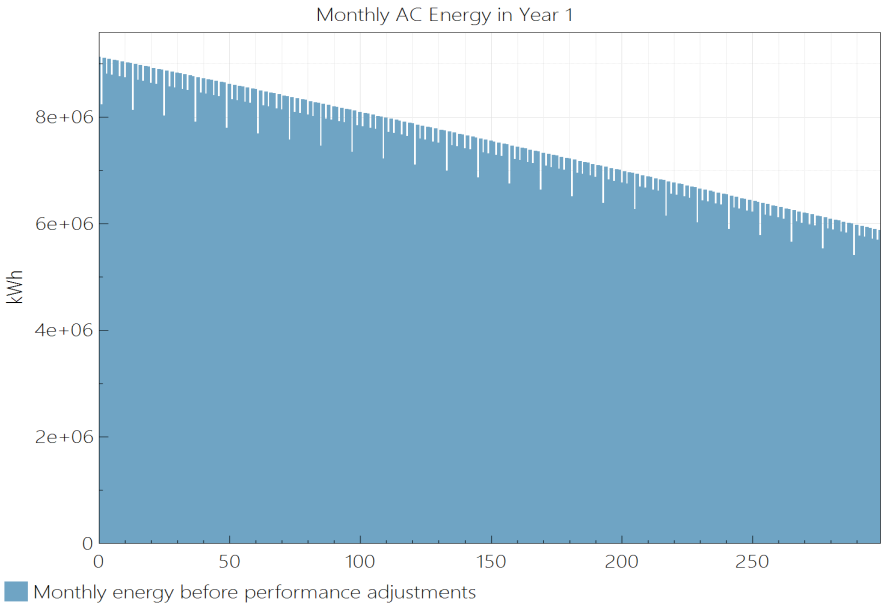

Figure 14. Monthly AC energy generation of the binary geothermal power plant at full capacity (Year 1).

Table 5. Performance metrics of the binary geothermal power plant at full capacity.

Metric	Value
Annual AC energy (year 1)	106,853,512 kWh
Capacity factor (year 1)	93.8%
PPA price in Year 1	8.00 ¢/kWh
PPA price escalation	1.00 %/year
LPPA Levelized PPA price nominal	8.61 ¢/kWh
LPPA Levelized PPA price real	6.95 ¢/kWh
LCOE Levelized cost of energy nominal	7.54 ¢/kWh
LCOE Levelized cost of energy real	6.09 ¢/kWh
NPV Net present value	9,901,763$
IRR Internal rate of return	32.2%
Year IRR is achieved	20
IRR at end of project	32.09%
Net capital cost	62,864,680$
Equity	20,169,926$
Size of debt	42,694,752$
Debt percent	67.92%

The comparative analysis further indicated that the binary configuration outperforms the flash technology under full-capacity operation. Consequently, the flash technology was excluded from the final analysis and discussion.

4.4. Cost Analysis

The cost analysis highlights clear differences in the economic feasibility of wind and geothermal power plants for desalination applications. At small-scale deployment, the LCOE of the geothermal power plant was calculated as 950.51 ¢/kWh for the binary technology and 933.85 ¢/kWh for the flash technology, whereas the wind power plant achieved a substantially lower LCOE of 41.16 ¢/kWh. This disparity is primarily due to the significantly higher fixed initial costs associated with geothermal powerplants compared to wind power plant. Geothermal power plant become more viable only when designed for larger power outputs and capacities.

When analyzed at full capacity, the binary geothermal power plant showed a dramatic improvement, with the LCOE dropping from 950.51 ¢/kWh to 6.09 ¢/kWh, clearly demonstrating the strong influence of economies of scale. In contrast, the integration of the flash technology proved infeasible under the given conditions, reinforcing the superiority of the binary configuration at higher capacities. For the wind power plant, the LCOE declined more gradually, from 41.16 ¢/kWh at small scale to 2.93 ¢/kWh at full capacity, indicating its economic stability and flexibility in scaling.

The financial performance indicators further confirm these trends. For the bi-

nary geothermal power plant, the IRR increased to 32% at full capacity, while the wind power plant improved from an IRR of –11.72% to 14%. These results illustrate that the scalability of wind power plant is more flexible than that of geothermal power plants; however, the binary geothermal plant benefits significantly from larger-scale deployment, where fixed costs are better distributed over higher energy outputs.

Overall, the analysis indicates that for meeting the energy demand of household-scale desalination systems, wind power plant represent the more economically feasible option due to their lower capital costs and more consistent cost reductions across scales. Nonetheless, the results also highlight that at sites with sufficient geothermal potential, binary geothermal power plants can achieve strong economic performance when operated at full capacity. Moreover, the selected locations for this study demonstrate promising potential for deploying both technologies at larger scales.

5. Conclusions

The SAM was employed to analyze the performance of wind turbine and geothermal systems for power generation to meet household desalination demands. As the free version of SAM was used, random site data were applied, and thus realistic values for Tripoli could not be directly obtained. The RO desalination system and its parameters were taken as a reference for the analysis. Given that the annual water requirement of 100 households was relatively small, the corresponding energy demand for desalination was also limited.

For the geothermal case, a binary plant operating at 180˚C with 80 % efficiency was modeled, while the wind energy system consisted of two Bergey Excel-S.60 turbines. The results revealed that wind velocity was generally higher from late night to early morning, leading to increased output during these hours. Seasonal variations were also evident, with the poorest wind turbine performance recorded during the summer months due to the lowest annual wind speeds. In contrast, geothermal output remained constant throughout the year, as expected for baseload energy. However, the geothermal power plant showed a decrease in capacity over time, while the wind turbine system exhibited only a modest decline.

The annual average energy generation was 3132 kW for the wind power plant and 3628 kW for the geothermal power plant, against an estimated demand of roughly 2395 kW. Despite meeting demand, the low-capacity requirement resulted in very high LCOE values, particularly for geothermal: 950.51 ¢/kWh for binary and 933.85 ¢/kWh for flash, compared to 41.16 ¢/kWh for wind.

A full-capacity analysis was therefore performed, considering an annual requirement of 3,802,082 kW. For wind energy, nine Siemens 3.6 MW turbines were modeled, while for binary geothermal power plant with two wells and a total capacity of 50 MW was evaluated. Under these conditions, the LCOE dropped significantly to 2.93 ¢/kWh for wind and 6.09 ¢/kWh for binary geothermal, demonstrating the strong effect of economies of scale. The flash technology, however, yielded lower outputs and unrealistic LCOE values compared to the binary tech-

nology, and was therefore excluded from the final analysis.

Overall, the results confirm that while small-scale geothermal deployment is economically unfeasible, binary geothermal power plants become highly competitive when operated at full capacity. Wind power plant, on the other hand, offer greater scalability and flexibility, with consistently favorable performance across both small and large scales. For the household desalination scenario considered in this study, wind energy represents the more practical and cost-effective option, while large-scale binary geothermal power plants remain a viable alternative in resource-rich locations.

Acknowledgements

This research work was supported by King Fahd University of Petroleum and Minerals (KFUPM) and Omar Al-Mukhtar University (OMU). The authors would also like to express their gratitude to both institutions for providing continuous support and research facilities that contributed to the success of this work.

Conflicts of Interest

The authors declare no conflicts of interest regarding the publication of this paper.

References

[1] Benali, M., Hamad, T. and Hamad, Y. (2019) Experimental Study of Biogas Production from Cow Dung as an Alternative for Fossil Fuels. *Journal of Sustainable Bioenergy Systems*, **9**, 91-97. https://doi.org/10.4236/jsbs.2019.93007

[2] Mohammed, M., Belkair, A., Hamad, T., Jirhiman, A., Hassan, R. and Ahmeedah, A. (2022) Improving Biogas Production from Animal Manure by Batch Anaerobic Digestion. *Algerian Journal of Engineering and Technology*, **60**, 79-84. https://jetjournal.org/index.php/ajet/article/view/199

[3] Mohammed, M., Hossain, M.M. and Bari, M.A.A. (2025) Optimizing Hard Carbon Anodes for Sodium-Ion Batteries: Effects of Pre-Treatment and Post-Treatment Techniques. *Battery Energy*, **4**, e70047. https://doi.org/10.1002/bte2.20250054

[4] Benali, M., Hamad, T., Belkhair, A. and Hamad, Y. (2019) Investigating the Use of Combined Hydrogen, Heat and Power System for Omar Al-Mukhtar University Campus. *Advances in Biological Chemistry*, **9**, 31-44. https://doi.org/10.4236/abc.2019.91003

[5] Kabiri, S., Khoshgoftar Manesh, M.H., Yazdi, M. and Amidpour, M. (2021) New Procedure for Optimal Solar Repowering of Thermal Power Plants and Integration with MSF Desalination Based on Environmental Friendliness and Economic Benefit. *Energy Conversion and Management*, **240**, Article ID: 114247. https://doi.org/10.1016/j.enconman.2021.114247

[6] Benali, M. (2019) Experimental Investigation of Biogas Production from Cow Dung in an Anaerobic Batch Digester at Mesophilic Conditions. *Iranica Journal of Energy & Environment*, **10**, 121-125.https://doi.org/10.5829/ijee.2019.10.02.09

[7] Adam, M., Abdalla, T., Mohammed, M., Bari, M.A.A. and Hossain, M.M. (2025) Fabrication, Characterization, and Applications of Hard Carbons: A Comprehensive Review. *Journal of Power Sources*, **652**, Article ID: 237674. https://doi.org/10.1016/j.jpowsour.2025.237674

[8] Prajapati, M., Shah, M. and Soni, B. (2022) A Comprehensive Review of the Geothermal Integrated Multi-Effect Distillation (MED) Desalination and Its Advancements. *Groundwater for Sustainable Development*, **19**, Article ID: 100808. https://doi.org/10.1016/j.gsd.2022.100808

[9] Benali, M., Hamad, T., Hamad, Y. and Belkhair, A. (2019) The Hydrogen Energy Potential of Solid Waste: A Case Study of Misrata City. *Advances in Biological Chemistry*, **9**, 45-53. https://doi.org/10.4236/abc.2019.92004

[10] Muetaz Mohammed, M.M., Boghandora, S.B., Hassan, R.H., Jirhiman, A.J. and Ali Ahmeedah, A.A. (2022) Influence of pH and the Insulation of Reactor on the Biogas Production of Livestock Waste by Batch Anaerobic Reactor. *Solar Energy and Sustainable Development Journal*, **11**, 1-12. https://doi.org/10.51646/jsesd.v11i2.140

[11] Ghaffour, N., Lattemann, S., Missimer, T., Ng, K.C., Sinha, S. and Amy, G. (2014) Renewable Energy-Driven Innovative Energy-Efficient Desalination Technologies. *Applied Energy*, **136**, 1155-1165. https://doi.org/10.1016/j.apenergy.2014.03.033

[12] Bozgeyik, A., Altay, L. and Hepbasli, A. (2022) A Parametric Study of a Renewable Energy Based Multigeneration System Using PEM for Hydrogen Production with and without Once-Through MSF Desalination. *International Journal of Hydrogen Energy*, **47**, 31742-31754. https://doi.org/10.1016/j.ijhydene.2022.02.186

[13] Gude, V.G., Nirmalakhandan, N. and Deng, S. (2011) Desalination Using Solar Energy: Towards Sustainability. *Energy*, **36**, 78-85. https://doi.org/10.1016/j.energy.2010.11.008

[14] Sayed, E.T., Olabi, A.G., Elsaid, K., Al Radi, M., Alqadi, R. and Ali Abdelkareem, M. (2023) Recent Progress in Renewable Energy Based-Desalination in the Middle East and North Africa MENA Region. *Journal of Advanced Research*, **48**, 125-156. https://doi.org/10.1016/j.jare.2022.08.016

[15] Greco, F., Heijman, S. and Jarquin-Laguna, A. (2021) Integration of Wind Energy and Desalination Systems: A Review Study. *Processes*, **9**, Article 2181. https://doi.org/10.3390/pr9122181

[16] Li, G. and Zhang, L. (2016) Investigation of a Solar Energy Driven and Hollow Fiber Membrane-Based Humidification-Dehumidification Desalination System. *Applied Energy*, **177**, 393-408. https://doi.org/10.1016/j.apenergy.2016.05.113

[17] Rafiei, A., Alsagri, A.S., Mahadzir, S., Loni, R., Najafi, G. and Kasaeian, A. (2019) Thermal Analysis of a Hybrid Solar Desalination System Using Various Shapes of Cavity Receiver: Cubical, Cylindrical, and Hemispherical. *Energy Conversion and Management*, **198**, Article ID: 111861. https://doi.org/10.1016/j.enconman.2019.111861

[18] Yıldırım, C. and Solmuş, İ. (2014) A Parametric Study on a Humidification-Dehumidification (HDH) Desalination Unit Powered by Solar Air and Water Heaters. *Energy Conversion and Management*, **86**, 568-575. https://doi.org/10.1016/j.enconman.2014.06.016

[19] Mohamed, A.M.I. and El-Minshawy, N.A.S. (2009) Humidification-Dehumidification Desalination System Driven by Geothermal Energy. *Desalination*, **249**, 602-608. https://doi.org/10.1016/j.desal.2008.12.053

[20] Caldera, U., Bogdanov, D. and Breyer, C. (2016) Local Cost of Seawater RO Desalination Based on Solar PV and Wind Energy: A Global Estimate. *Desalination*, **385**, 207-216. https://doi.org/10.1016/j.desal.2016.02.004

[21] Shahbazi, R., Kouravand, S. and Hassan-Beygi, R. (2019) Analysis of Wind Turbine Usage in Greenhouses: Wind Resource Assessment, Distributed Generation of Electricity and Environmental Protection. *Energy Sources, Part A: Recovery, Utilization*,

and Environmental Effects, **45**, 7846-7866.
https://doi.org/10.1080/15567036.2019.1677810

[22] Mojtahedzadeh, N., Ghalandarzadeh, A. and Motamed, R. (2021) Experimental Evaluation of Dynamic Characteristics of Firouzkooh Sand Using Cyclic Triaxial and Bender Element Tests. *International Journal of Civil Engineering*, **20**, 125-138.
https://doi.org/10.1007/s40999-021-00644-6

[23] Pourasl, H.H., Barenji, R.V. and Khojastehnezhad, V.M. (2023) Solar Energy Status in the World: A Comprehensive Review. *Energy Reports*, **10**, 3474-3493.
https://doi.org/10.1016/j.egyr.2023.10.022

[24] Ahmed, F.E., Hashaikeh, R. and Hilal, N. (2019) Solar Powered Desalination—Technology, Energy and Future Outlook. *Desalination*, **453**, 54-76.
https://doi.org/10.1016/j.desal.2018.12.002

[25] Shelare, S., Kumar, R., Gajbhiye, T. and Kanchan, S. (2023) Role of Geothermal Energy in Sustainable Water Desalination—A Review on Current Status, Parameters, and Challenges. *Energies*, **16**, Article 2901. https://doi.org/10.3390/en16062901

[26] Zarzo, D. and Prats, D. (2018) Desalination and Energy Consumption. What Can We Expect in the near Future? *Desalination*, **427**, 1-9.
https://doi.org/10.1016/j.desal.2017.10.046

[27] Hamad, S. and Fensham, R. (2025) Groundwater: An Important Resource of Urban Water Supply in Libya. In: Zurqani, H.A., Ed., *Water Resources of Libya*, Springer, 41-66. https://doi.org/10.1007/978-3-031-80920-0_3

[28] Fanack Water (2023) Domestic Water Uses in Libya Varies Greatly. Fanack Water Report. https://water.fanack.com/libya/water-uses-in-libya

[29] De Araujo, J.M.S. (2019) WRF Wind Speed Simulation and SAM Wind Energy Estimation: A Case Study in Dili Timor Leste. *IEEE Access*, **7**, 35382-35393.
https://doi.org/10.1109/access.2019.2904755